A Numerical Investigation of the Effects of Dry Air Aloft on Deep Convection

RICHARD P. JAMES AND PAUL M. MARKOWSKI

Department of Meteorology, The Pennsylvania State University, University Park, Pennsylvania

(Manuscript received 27 March 2009, in final form 2 July 2009)

ABSTRACT

A three-dimensional cloud model was used to investigate the sensitivity of deep convective storms to dry air above the cloud base. In simulations of both quasi-linear convective systems and supercells, dry air aloft was found to reduce the intensity of the convection, as measured by updraft mass flux and total condensation and rainfall. In high-CAPE line-type simulations, the downdraft mass flux and cold pool strength were enhanced at the rear of the trailing stratiform region in a drier environment. However, the downdraft and cold pool strengths were unchanged in the convective region, and were also unchanged or reduced in simulations of supercells and of line-type systems at lower CAPE. This result contrasts with previous interpretations of the role of dry air aloft in the development of severe low-level outflow winds.

The buoyancy-sorting framework is used to interpret the influence of environmental humidity on the updraft entrainment process and the observed strong dependence on the environmental CAPE. The reduction in convective vigor caused by dry air is relatively inconsequential at very high CAPE, but low-CAPE convection requires a humid environment in order to grow by entrainment.

The simulated responses of the downdraft and cold pool intensities to dry air aloft reflected the changes in diabatic cooling rates within the downdraft formation regions. When dry air was present, the decline in hydrometeor mass exerted a negative tendency on the diabatic cooling rates and acted to offset the favorable effects of dry air for cooling by evaporation. Thus, with the exception of the rearward portions of the high-CAPE line-type simulations, dry air was unable to strengthen the downdrafts and cold pool.

A review of the literature demonstrates that observational evidence does not unambiguously support the concept that dry air aloft favors downdraft and outflow strength. It is also shown that the use of warm rain microphysics in previous modeling studies may have reinforced the tendency to overemphasize the role of dry air aloft.

1. Introduction

In recent decades numerous studies have examined the sensitivity of deep convection to both thermodynamic and kinematic properties of the larger-scale environment within which the convection exists. Certain key environmental properties have been found to exert strong and predictable influences on the structure and evolution of convection, including vertical wind shear (e.g., Thorpe et al. 1982), convective available potential energy (CAPE; e.g., Weisman and Klemp 1982) and the height of the lifting condensation level (McCaul and Cohen 2002). The investigation of environmental influences on deep convection has proven to be highly fruitful, despite the practical difficulty of strictly defining the convective environment (Brooks et al. 1994; Markowski and Richardson 2007).

An aspect of the convective environment that is frequently cited in relation to midlatitude severe thunderstorms is the relative humidity of the air above the cloud base. In the severe storms literature, low relative humidity in the lower or middle troposphere above the cloud base is generally regarded as favorable for the formation of strong evaporatively driven downdrafts (Johns and Doswell 1992; Gilmore and Wicker 1998). Consequently, dry air aloft is often perceived by forecasters as an ingredient for the production of damaging straight-line winds, particularly in widespread episodes known as derecho events (Johns and Hirt 1987). Thus, in the context of midlatitude storms, the role of dry air aloft is interpreted primarily as influencing the downdraft-forming process. However, in the literature on tropical convection, environmental humidity is most often discussed in terms of its effects on the updraft entrainment

Corresponding author address: Richard P. James, Prescient Weather Ltd., 200 Innovation Blvd., Ste. 257, State College, PA 16801. E-mail: rpj105@earthlink.net

DOI: 10.1175/2009MWR3018.1

process. The presence of dry air in the environment of convective updrafts is believed to be detrimental to convective intensity, and the environmental humidity has been recognized as an important factor in the regulation of convective activity over the tropical oceans (Brown and Zhang 1997; Parsons et al. 2000). A contrast therefore exists between the most widespread perceptions of the influences of dry air on midlatitude and tropical convection. This study seeks to clarify the effects of dry air aloft on deep convection by using a high-resolution numerical model to conduct idealized sensitivity tests.

In elucidating the effects of environmental humidity, it is useful to distinguish between the direct effects of surrounding dry air on convective overturning and the ''indirect'' effects that only become apparent when lifting is applied to the environment. If dry air resides above relatively moist air, then lifting can result in efficient destabilization as the lapse rate and CAPE increase; this process is known to be important in some convective events (Carr and Millard 1985). However, a uniformly moist environment is unable to experience significant destabilization from lifting. Thus, dry air aloft can be regarded as indirectly influencing convection by regulating the effects of vertical motion on the stability of the environment. Although the lifting of dry air may be a crucial element in some convective scenarios, this study seeks to examine only the direct effects of dry air in the absence of externally imposed vertical motion. Further research is needed to quantify the relative magnitudes of dry air–regulated stability changes and the direct effects discussed here.

Although the presence of unusually dry (or moist) air in the environment of strong convective storms has been addressed peripherally in a number of past modeling efforts, there have been few rigorous investigations of the subject. In an oft-cited study, Gilmore and Wicker (1998) simulated supercell thunderstorms in environments having dry layers of varying strength and height and found that low-level cold outflow within the first hour was considerably enhanced when dry air was present aloft, except when the dry air was located above 3 km and the wind shear was greater than 50 m s^{-1} over 6.7 km. Dry air aloft led to a greater propensity for outflow-dominated supercells, and overall storm intensity, as measured by maximum vertical velocity, was reduced substantially after the first hour. Gilmore and Wicker (1998) concluded that downdraft strength is enhanced by dry air aloft, but suggested that their experiments should be repeated with ice microphysics.

This study discusses simulations of both quasi-linear convective (''line type'') systems and supercells in which the sensitivity to dry air above the cloud base was tested. Section 2 describes the modeling framework that was used, section 3 discusses the results, and section 4 addresses the interpretation of the existing literature in view of the new results.

2. Methodology

a. Model setup

The cloud-simulating model of Bryan and Fritsch (2002) and Bryan (2002) was used in this study; this model has been used in previous idealized modeling studies (e.g., Bryan et al. 2006; Kirshbaum et al. 2007). The numerical model was configured to solve the compressible governing equations in a three-dimensional framework, using a horizontally homogeneous base state into which one or more warm, moist bubbles was introduced to initiate convection. The sensitivity to environmental moisture was tested by systematically altering the vertical structure of the base state as described below. Simulations were run for 6 h in the line-type simulations, with horizontal and vertical grid spacings of 400 and 250 m, respectively. The supercell simulations were run for 2 h, using a horizontal grid spacing of 250 m, and a vertical grid spacing that expanded from 125 m at the ground to 250 m above 7.5 km.

The integration of the governing equations was accomplished using the Runge–Kutta technique as formulated for compressible models (Wicker and Skamarock 2002), with fifth-order spatial discretization and no additional artificial diffusion. The subgrid turbulence parameterization is based on the turbulence kinetic energy scheme of Deardorff (1980). Unless otherwise stated, the National Aeronautics and Space Administration (NASA) Goddard version of the Lin et al. (1983) microphysical scheme was used (Braun and Tao 2000), with hail selected as the large ice category; this scheme represents five species of water condensate (cloud droplets, cloud ice particles, rain, snow, and hail). The Coriolis force was not included, and no surface fluxes or radiative heating were included.

In the line-type simulations, the geometry of the convection was accommodated by using a model domain that extended for 80 km in the along-line direction and 400 km in the across-line direction. The lateral boundary conditions were periodic in the along-line direction and open radiative in the across-line direction. The domain size for the supercell simulations was 120 km $\times$ 100 km, the longer dimension being the direction of the upper-level wind, and in these experiments open-radiative boundary conditions were used on all lateral boundaries. The top and bottom boundaries of the domain were flat in all cases, with free-slip boundary conditions; the vertical size of the domain was 20 km, and a Rayleigh damping

layer was applied above 16 km to reduce the reflection of gravity waves from the upper boundary.

Convection was initialized in the squall-line simulations with a line of bubbles having a positive temperature and water vapor perturbation, spaced 20 km apart across the short dimension of the model domain. The bubbles were placed 2.5 km above ground, with a maximum temperature perturbation in each bubble of 3 K, and a maximum relative humidity of 95%. The supercell simulations were initialized with a single bubble having the same characteristics. Random potential temperature fluctuations of magnitude up to 0.1 K were included in the initial state throughout the domain.

b. Base-state sounding generation

Base-state soundings were constructed using separate methods for the line-type and supercell simulations. In the simulations of quasi-linear systems, it was desirable to explore a broad range of CAPE values, leading to the use of the technique of James et al. (2006), which builds upon the approach of McCaul and Weisman (2001). Using this method, the shape of the vertical profile of buoyancy can be preserved in environments having varying CAPE. The analytic form of the buoyancy profile is given in James et al. (2006); line-type convection was simulated in environments having CAPE of 1500, 3000, and 4500 J kg^{-1}. The profile compression parameter m was set to 0.8 when the CAPE was 3000 or 4500 J kg^{-1}, implying maximum parcel buoyancy at 6.9 km above the top of the surface-based mixed layer. However, when the CAPE was 1500 J kg^{-1}, using this value of m required undesirably large perturbations at initialization to generate long-lived quasi-linear systems; therefore m was raised to 3.2 in the low-CAPE simulations, corresponding to maximum buoyancy at 3.9 km above the mixed layer top. The vertical scale height H was 12.75 km, and the equilibrium level and tropopause were placed 13.0 and 11.0 km, respectively, above the top of the mixed layer.

In all of the line-type simulations, the mixed layer top was placed at the height of the fifth model level at 1.125 km above ground level (AGL), and the conditions at the mixed layer top were specified by a pressure of 900 hPa, relative humidity of 95%, and equivalent potential temperature (θ_e) of 345 K. The temperature and mixing ratio profiles in the mixed layer were then obtained by assuming that θ_e was constant and that the potential temperature increased with height at a rate of 1 K km^{-1}. The latter constraint was chosen to prevent shear-generated mixing in the boundary layer; thus, the subcloud layer was not truly well mixed, but it is nevertheless referred to as the ''mixed layer'' herein.

For the control simulations of the line-type systems, the relative humidity in the troposphere above the mixed layer top was specified according to the analytic profile:

$$H = 0.95 - 0.45\left(\frac{z - z_{\text{mix}}}{z_{\text{trop}} - z_{\text{mix}}}\right)^{0.7}, \qquad (1)$$

where z is the height above ground, z_{trop} is the height of the tropopause, and z_{mix} is the height of the mixed layer top. The effects of varying midtropospheric humidity were then investigated by introducing to the base state a domain-wide layer spanning seven model levels (1.5 km) in which the relative humidity was reduced; the height of the center of the dry layer was initially set to 3.375 km AGL. At the five model levels in the center of the dry layer, the relative humidity was reduced to 10%, and at the top and bottom level within the dry layer, the relative humidity was reduced halfway to 10%. Additional experiments were performed using the low-CAPE (1500 J kg^{-1}) sounding in which the relative humidity was reduced only to 50% and to 70% in the dry layer. Within the dry layer, the temperature was adjusted to preserve the virtual temperature that was specified by the analytic buoyancy profile; thus, the CAPE and the vertical distribution of buoyancy were unchanged in the sensitivity tests with dry air. Two pairs of base states having CAPE of 4500 and 1500 J kg^{-1} respectively are shown in Figs. 1 and 2.

The control base state in the supercell simulations employed the analytic sounding of Weisman and Klemp (1982) with a low-level mixing ratio of 14 g kg^{-1}, in order to facilitate comparison with previous studies. As in the line-type simulations, a dry layer was introduced for the sensitivity test; however, owing to the smaller vertical grid spacing, the dry layer spanned 9 model levels (1.54 km) and was centered at 3.39 km AGL.

In the simulations of the quasi-linear convective mode, the base-state wind profile contained line-perpendicular shear only in the lowest 2.5 km, and zero along-line winds; this shear profile is typical of many squall-line studies. For the soundings with CAPE of 4500 J kg^{-1}, the magnitude of the shear was 17.5 m s^{-1}, but for lower values of CAPE the shear was 10 m s^{-1} to facilitate the development of an upshear-tilted mode of organization. The supercell experiments employed the quarter-circle supercell hodograph of Weisman and Rotunno (2000); the 0–6-km length of the hodograph was 35 m s^{-1}, with constant winds above 6 km; the bulk Richardson number (Weisman and Klemp 1982) was 27.

3. Results

a. Quasi-linear convective systems

In each of the simulations initialized with a line of warm bubbles, a long-lived convective system was generated,

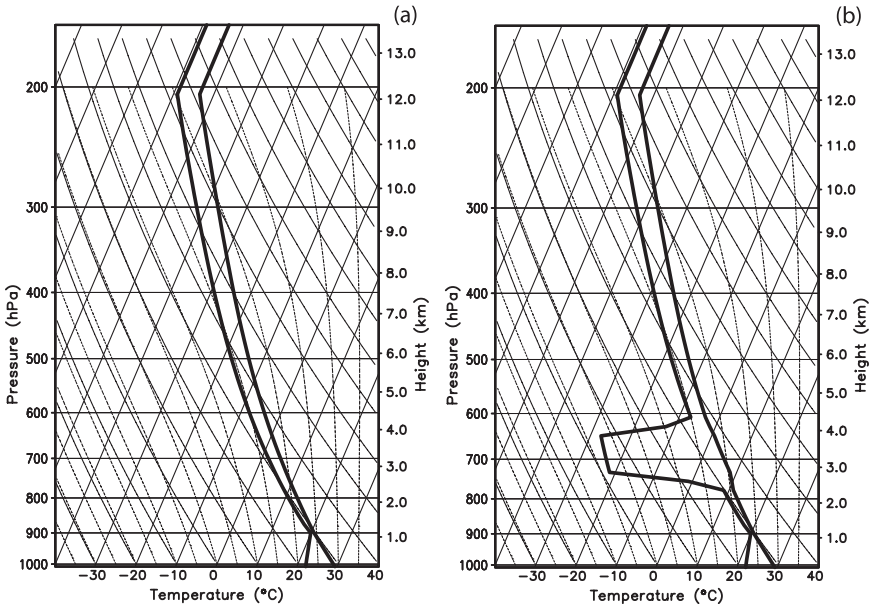

FIG. 1. Base-state soundings with CAPE of 4500 J kg^{-1} for (a) the control (moist) relative humidity profile and (b) having a dry layer centered at 3.375 km AGL with minimum relative humidity of 10%.

consisting of a quasi-linear region of deep convective updrafts and downdrafts oriented perpendicular to the wind shear, and a trailing stratiform region that expanded rearwards in a shear-relative sense. The evolution of the systems over the 6-h duration of each simulation was consistent with previous conceptual models of squall-line evolution (Weisman et al. 1988; Lafore and Moncrieff 1989). However, significant differences were observed between environments having different stability and humidity characteristics. In the discussion that follows, the simulations having a dry layer in the base state will be referred to as ''dry'' simulations, whereas simulations not having a dry layer will be called ''moist'' simulations. The terms ''high-CAPE,'' ''moderate-CAPE,''

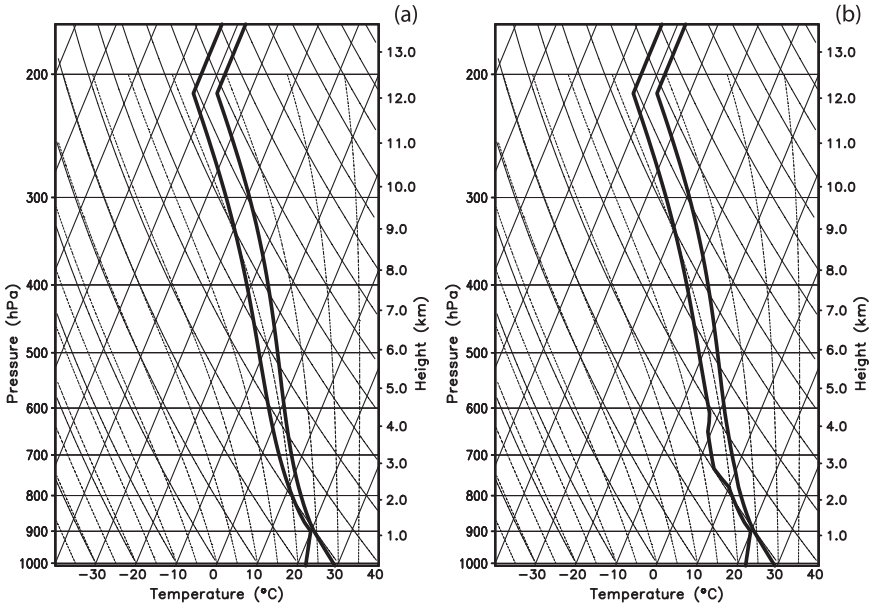

FIG. 2. As in Fig. 1, but for a CAPE of 1500 J kg^{-1} and with minimum relative humidity of 70%.

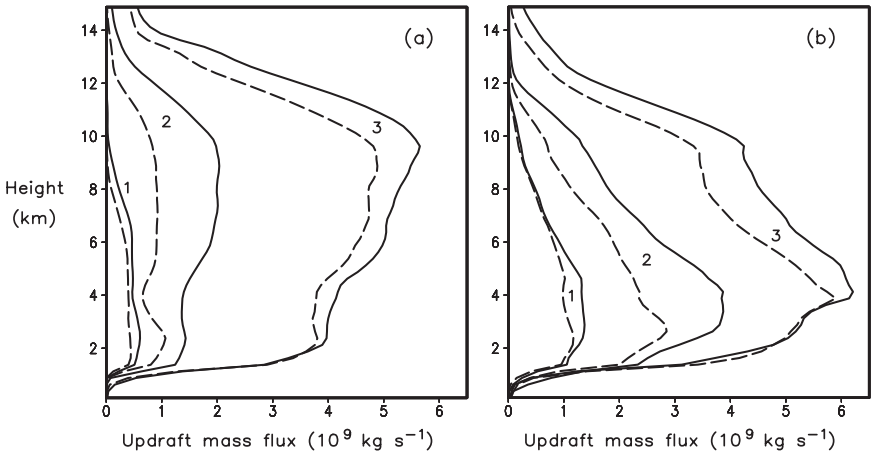

FIG. 3. Updraft mass flux at (a) 2 and (b) 5 h in the line-type simulations having CAPE of (1) 1500, (2) 3000, and (3) 4500 J kg^{-1}. The solid lines depict results for the moist simulations and the dashed lines show results for the dry simulations. For the dry simulation with CAPE of 1500 J kg^{-1}, the relative humidity in the dry layer was reduced to only 70%; the dry layers in the higher-CAPE simulations contained 10% relative humidity.

and "low-CAPE" will refer to the environments having CAPE of 4500, 3000, and 1500 J kg^{-1}, respectively.

1) UPDRAFT PROCESSES

The effect of dry environmental air on the updraft mass flux in the line-type simulations is shown in Fig. 3. For the purpose of defining an updraft, Cohen (2000) was followed (i.e., a grid point was classified as an updraft point if the vertical velocity was greater than 0.5 m s^{-1} and the sum of the cloud water and cloud ice mixing ratios was greater than 0.01 g kg^{-1}). In every experiment, the updraft mass flux was reduced in the presence of dry air through most of the depth of the troposphere. In the low-CAPE environment, a dry layer having relative humidity of 10% was so detrimental that a long-lived convective system was unable to develop; thus, the dry result shown in Fig. 3 for CAPE of 1500 J kg^{-1} represents the mass flux when the dry layer humidity was reduced to only 70%. In this case, a very modest decrease in humidity (cf. Figs. 2a,b) still caused a significant drop in updraft mass flux.

The low-level (sub-2-km AGL) updraft mass flux exhibited a different sensitivity to dry air aloft, because in the mature stages of the convective systems, the low-level ascent was dominated by forced lifting above the leading edge of the surface-based cold pool. The low-level mass flux therefore varied in response to changes in the cold pool strength. In the high-CAPE simulations, the cold pool strength was similar within its leading portion in the moist and dry environments, and thus the low-level updraft mass flux was largely unchanged when dry air was present. However, at lower values of CAPE, the cold pool intensified more slowly and tended to be weaker in the dry simulations, leading to a modest reduction in the updraft mass flux at low levels. Cold pool characteristics are discussed further in section 3a(2).

The distinction between the low-level dynamically forced lifting and the midlevel buoyancy-driven ascent is evident in Fig. 4, which depicts an along-line average of the vertical mass flux for the mature stages of the high-CAPE simulations. Immediately above the gust front is an updraft mass flux maximum associated with the intense slablike lifting at the leading edge of the cold pool; the secondary maximum in updraft mass flux between 3 and 10 km above ground and 10–20 km rearward of the gust front is caused by buoyancy-driven ascent. A very similar structure in the mass flux cross section was present in all of the line-type simulations in their mature stages. Dry air was observed to weaken the midlevel updraft maximum in every instance compared to the corresponding moist simulation. When the CAPE was 3000 J kg^{-1} or less, the low-level updraft maximum was also reduced in strength, but in the high-CAPE simulations the low-level maximum was largely unchanged.

Alternative measures of the overall convective intensity are provided by the total condensation and rainfall, which were consistently reduced in the presence of dry air (Fig. 5). The total mass of each species of condensate was also reduced (not shown). The sensitivity of the domain-wide maximum vertical velocity was also examined, and it was found that dry air caused little change to the largest updraft velocities in the mature stages of the long-lived convective systems. In the first 2–3 h of the simulations, however, the peak updraft velocities tended to be weakened by dry air, especially under low-CAPE conditions.

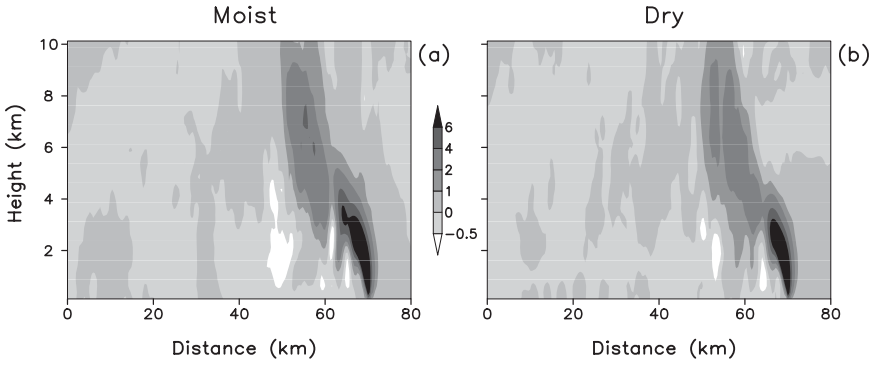

FIG. 4. Along-line average of the mass flux (kg m^{-2} s^{-1}) at 5 h in the (a) moist and (b) dryline-type simulations having CAPE of 4500 J kg^{-1}. The along-line average is calculated with respect to the position of the gust front.

The effect of dry air on updrafts is further evident in the distribution of θ_e at updraft grid points between 6 and 9 km AGL (Fig. 6). In the drier environments, the θ_e distribution was shifted to lower values, reflecting the presence of drier environmental air that was entrained into the updrafts. Also notable is the higher median of the distribution at lower CAPE, resulting from the much lower entrainment rate in the less unstable environment; the entrainment process is discussed further below.

It should be noted that all of the long-lived convective systems retained their quasi-linear morphology throughout the simulations, and that the presence of dry air did not cause significant differences in organizational mode. This is illustrated by Fig. 7, which shows the lowest-level rain mixing ratio and wind, as well as the vertical velocity at 6 km AGL, at 3 h in the high- and moderate-CAPE simulations. When the sounding included dry air, the convective mode was unchanged, but the rainfall rate was reduced and the midlevel updrafts were reduced in size; the effect was much more pronounced at lower CAPE.

In each of the measures of convective intensity, a clear sensitivity to CAPE was observed in the effects of dry air aloft. When the CAPE was 4500 J kg^{-1}, the overall intensity of the convection was reduced modestly, but the influence of dry air was relatively minor. However, in the lower-CAPE environments, dry air caused a much more significant decrease in convective intensity. As previously noted, when the CAPE was 1500 J kg^{-1}, a long-lived convective system was precluded altogether when the relative humidity in the dry layer was 10%; the same was true for a dry layer with relative humidity of 50%. The dramatic sensitivity of the domain-wide total condensate mass to the dry layer humidity is shown in Fig. 8. A dry layer having relative humidity of 70% (Fig. 2b) caused a reduction in condensate mass of approximately 25% at times after 1.5 h, but a reduction to 50% humidity or lower led to the rapid demise of the convection. In response to a suggestion by an anonymous reviewer, the simulation with 50% humidity in the dry layer was repeated with reduced vertical grid spacing of 150 m; this change caused an even more rapid decay of the convection after 2 h, suggesting that the inability to sustain convection in the dry environments was not caused by insufficient vertical resolution.

The reduction in the midlevel updraft mass flux, the condensation rate, and the condensate mass in a dry environment reflects the well-known effects of environmental dry air on updraft growth through entrainment.

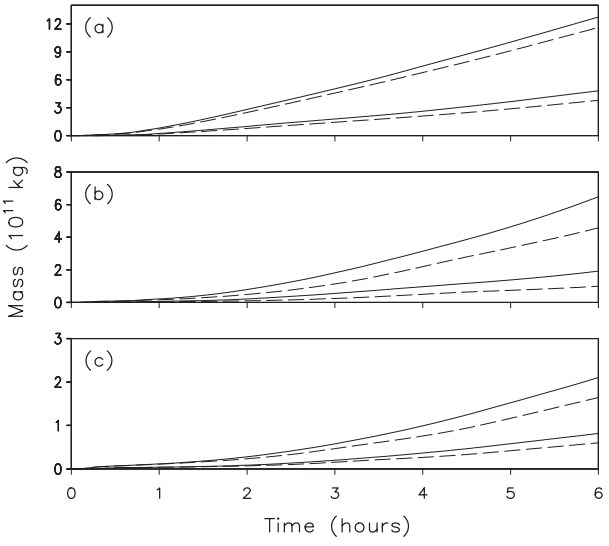

FIG. 5. Domain-wide total condensation and rainfall for the moist (solid lines) and dry (dashed lines) line-type simulations having CAPE of (a) 4500, (b) 3000, and (c) 1500 J kg^{-1}. The top pair of lines shows the condensation and the bottom pair of lines shows the rainfall. For the dry simulation with CAPE of 1500 J kg^{-1}, the relative humidity in the dry layer was reduced to only 70%; the dry layers in the higher-CAPE simulations contained 10% relative humidity.

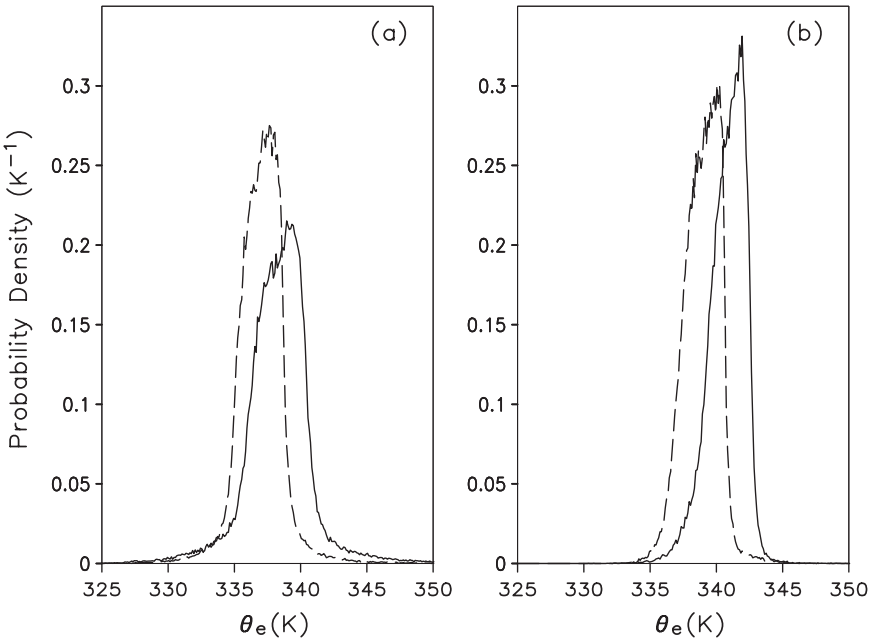

FIG. 6. Probability density function of equivalent potential temperature within updrafts between 6 and 9 km AGL at 5 h in the moist (solid lines) and dry (dashed lines) line-type simulations having CAPE of (a) 4500 and (b) 3000 J kg^{-1}.

As discussed by Kain and Fritsch (1990), for example, reduced environmental humidity causes greater evaporative cooling when cloud air mixes with environmental air, so that a mixture of cloud and environmental air is less likely to be positively buoyant. In a moist environment, by contrast, most mixtures are positively buoyant. Thus, according to the buoyancy-sorting model of Raymond and Blyth (1986) and Kain and Fritsch (1990), the rate of entrainment is enhanced when the environmental humidity is relatively high.

To illustrate the dependence of the mixing process on the environmental humidity, and to understand the sensitivity to CAPE that was observed in the simulations, a simple calculation of mixed parcel properties was performed. Figure 9 shows the density temperature perturbation of mixed air arising from the mixing of updraft and environmental air in varying fractions. The density temperature (Emanuel 1994) is defined by

$$T_\rho = T\left[\frac{1 + (q_v/\varepsilon)}{1 + q_t}\right], \qquad (2)$$

where T is the temperature, q_v is the water vapor mixing ratio, ε is the ratio of the specific gas constants of dry air and water vapor, and q_t is the total water mixing ratio. The density temperature perturbation is defined relative to the density temperature of the base state, and is directly proportional to the thermal buoyancy (Doswell and Markowski 2004). The mixed parcel properties were derived from the weighted combinations of the moist enthalpy and total water mixing ratio of the updraft and environmental air; both of these quantities are conserved in the idealized (isobaric, closed system) process (Emanuel 1994). For the calculations shown in Fig. 9, the updraft air was assumed to contain liquid water with a mixing ratio of 2 g kg^{-1}, and the updraft density temperature perturbation was 2.0 K. An environmental temperature of 270 K was used, and the pressure was 700 hPa. Figure 9 shows that lower environmental humidity expands the range of mixing fractions resulting in negative buoyancy; conversely, positive buoyancy in the mixed parcel is restricted to smaller fractions of environmental air. This suggests that fewer mixing events result in positive buoyancy when dry air is present, although the probability distribution of mixing fractions in a real cloud is uncertain (Cohen 2000) and could itself depend on the environmental humidity. Neglecting the possible sensitivity of the distribution of mixing fractions to environmental conditions, the simple calculations depicted in Fig. 9 confirm the notion that drier environmental air reduces the likelihood of a mixed parcel attaining positive buoyancy and therefore being entrained into the updraft.

The mixing calculations were repeated for updraft parcels having a range of T_ρ perturbations from 0 to 5 K, and for environmental air having a range of relative

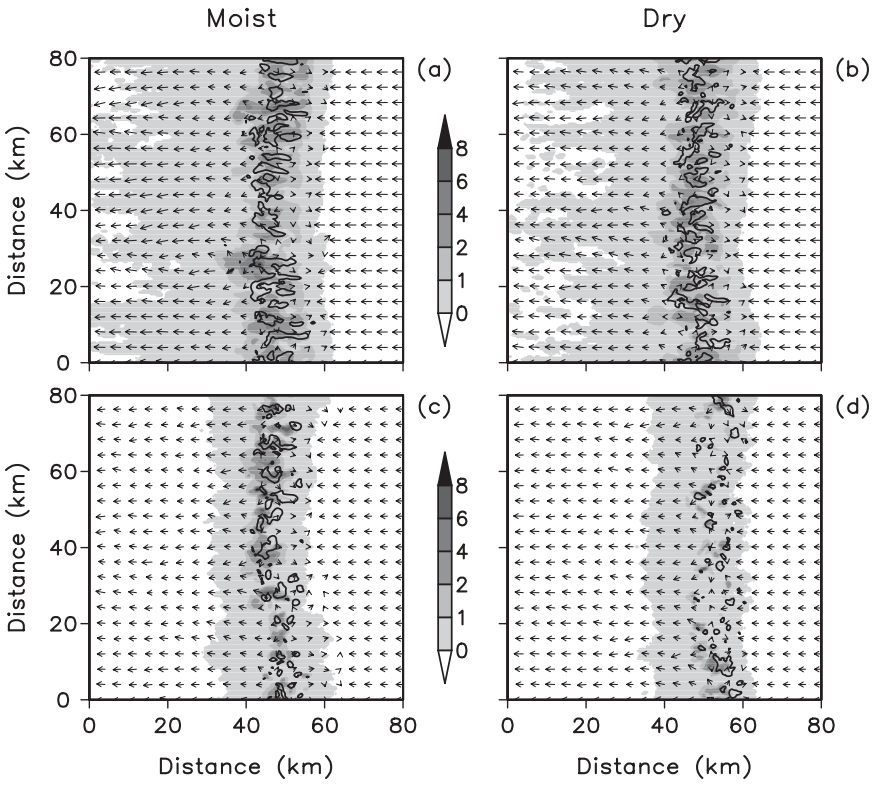

FIG. 7. Rain mixing ratio (g kg^{-1}, shaded) and lowest-level wind vectors at every 10th grid point (arrow length of 5 km corresponds to a wind speed of 40 m s^{-1}) at 0.125 m AGL, and the 10 m s^{-1} isopleth of vertical velocity (solid line) at 6 km AGL, at 3 h in the (a),(c) moist and (b),(d) dry line-type simulations having CAPE of (a),(b) 4500 and (c),(d) 3000 J kg^{-1}.

humidity from 0% to 100%. For each combination of updraft density temperature and environmental humidity, the maximum fraction of environmental air resulting in positive buoyancy in the mixed parcel was obtained. The maximum buoyant fraction for all updraft–environment combinations is shown in Fig. 10. As expected, lower environmental humidity causes a reduction in the maximum buoyant fraction, for all updrafts having a T_ρ perturbation below approximately 4.1 K. Above this temperature, no amount of mixing can render the updraft air negatively buoyant, because the complete evaporation of liquid water from the updraft fraction provides insufficient cooling; thus, all mixtures would be entrained in the buoyancy-sorting model.

Figure 10 also clearly shows that a change in environmental humidity from near 100% to a lower value causes a larger reduction in the range of positively buoyant mixing fractions when the updraft temperature perturbation is lower. For example, a drop in relative humidity from 95% to 70% reduces the maximum buoyant fraction from 0.8 to 0.4 when the updraft T_ρ perturbation is 1 K; in this case, dry air would be expected to significantly reduce the rate of entrainment. For an updraft T_ρ perturbation of 3.5 K, the same drop in relative humidity reduces the maximum buoyant fraction from approximately 0.95 to 0.72, implying a less severe reduction in entrainment rate. Updraft air parcels having T_ρ perturbations above 4.1 K remain positively buoyant regardless of the amount of mixing.

Using this simple model of the mixing process, a qualitative understanding of the observed sensitivity to CAPE is obtained. Assuming a comparable vertical profile of buoyancy (as in the analytic soundings used here), relatively high CAPE implies that the average buoyancy of updraft parcels is higher at each level. The probability of a mixing event leading to negative buoyancy is therefore reduced, and the rate of entrainment is enhanced compared to a low-CAPE scenario. Moreover, the presence of dry air causes a smaller reduction in the entrainment rate when CAPE is high, as the range of positively buoyant mixing fractions remains relatively high. Convection in a high-CAPE environment is therefore better able to withstand the detrimental effects of dry air, as the entrainment rate is less sensitive to low environmental humidity. Conversely, low-CAPE convection is highly dependent on having a humid environment in

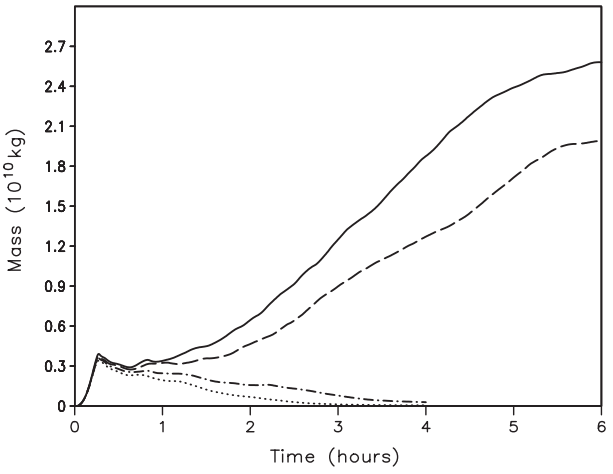

FIG. 8. Total condensate mass in the line-type simulations having CAPE of 1500 J kg^{-1}, for the moist simulation (solid line) and the simulations having a dry layer with relative humidity of 70% (dashed line), 50% (dash–dot line), and 10% (dotted line).

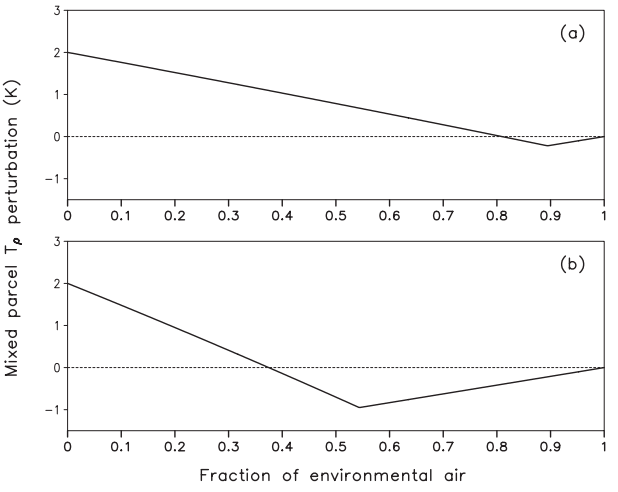

FIG. 9. Mixed parcel density temperature perturbation arising from the mixing of updraft and environmental air in varying fractions. The updraft air has a density temperature perturbation of 2 K at a pressure of 700 hPa, and contains liquid water with a mixing ratio of 2 g kg^{-1}. The environmental air has a temperature of 270 K, with a relative humidity of (a) 90% and (b) 30%.

order to grow by entrainment. This distinction may explain why tropical convection is widely perceived as being weakened when dry air is present, whereas midlatitude convection, which often benefits from much higher CAPE, is not typically regarded as being hindered by dry air aloft.

The results reported here are consistent with previous modeling studies (e.g., Kain and Fritsch 1990; Cohen 2000), and with observational work (e.g., Brown and Zhang 1997; Parsons et al. 2000). An important distinction, however, is that the results of this study are relevant specifically to the effect of midlevel relative humidity, in the absence of any significant changes to CAPE or convective inhibition (CIN). Some previous investigations have discussed the effects of tropical dry intrusions in terms of the accompanying increase in CIN (Parsons et al. 2000) or reduction in the depth of the near-surface layer of high θ_e (Kingsmill and Houze 1999). Similarly, Cohen (2000) attributed the benefits of increased humidity partially to the deepening of the near-surface layer of positive CAPE. In all of the sensitivity tests reported in this section, however, the CAPE of air parcels originating at or below 2.625 km AGL was identical in the moist and dry simulations. The vertically integrated CAPE (ICAPE; Mapes 1993) was also unchanged to within 2% in these simulations, showing that dry air hinders updraft growth by processes other than the reduction of the CAPE of potentially buoyant parcels.

2) DOWNDRAFT PROCESSES

The along-line averaged structure of the downdraft mass flux in the line-type simulations with moderate and high CAPE is depicted in Figs. 11 and 12. In the early stages of the simulations, the downdraft mass flux was concentrated in a narrow zone immediately behind the intense updrafts at the leading edge of each system, with a peak magnitude below 3 km AGL. As the convective systems matured, the downdraft mass flux weakened in this "forward zone," and a secondary maximum in downdraft mass flux (the "rearward zone") developed at the rear edge of the stratiform region, with a peak mass flux

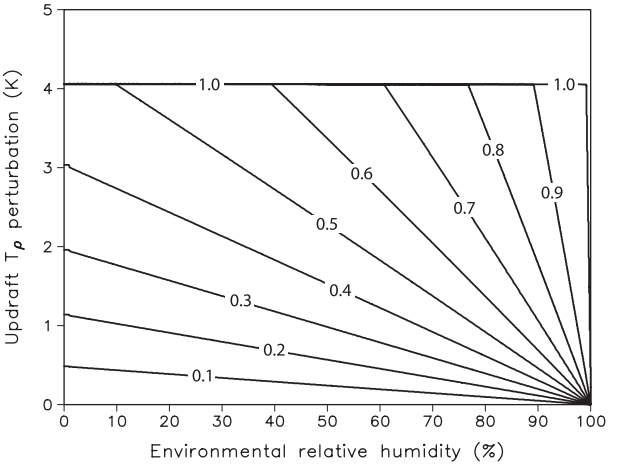

FIG. 10. Maximum fraction of environmental air that results in positive buoyancy when updraft and environmental air are mixed. As an example, the maximum buoyant fraction for the updraft–environment combination depicted in Fig. 9a is 0.81. The updraft air contains liquid water with a mixing ratio of 2 g kg^{-1}; the environmental air has a temperature of 270 K and the pressure is 700 hPa.

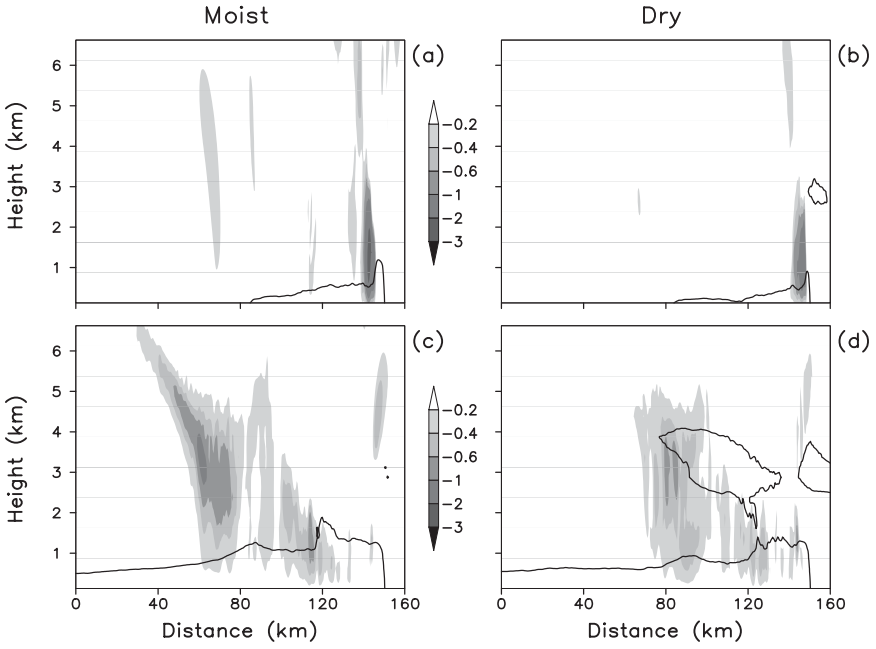

FIG. 11. Along-line average of the mass flux (shaded, kg m^{-2} s^{-1}) at (a),(b) 2 and (c),(d) 5 h in the (a),(c) moist and (b),(d) dry line-type simulations with CAPE of 3000 J kg^{-1}. The solid line depicts the −1 K contour of the along-line averaged potential temperature perturbation.

between 2 and 4 km AGL. The two distinct regions of downdraft formation are a characteristic feature of mature squall lines, as documented by Zipser (1977).

When dry air was present in the moderate-CAPE environment, the downdraft mass flux was reduced in both the forward and rearward zones (Fig. 11); the same effect was observed in the low-CAPE simulations (not shown). However, when the CAPE was 4500 J kg^{-1}, the rearward downdrafts were enhanced slightly in the drier environment in the mature stages of the convection,

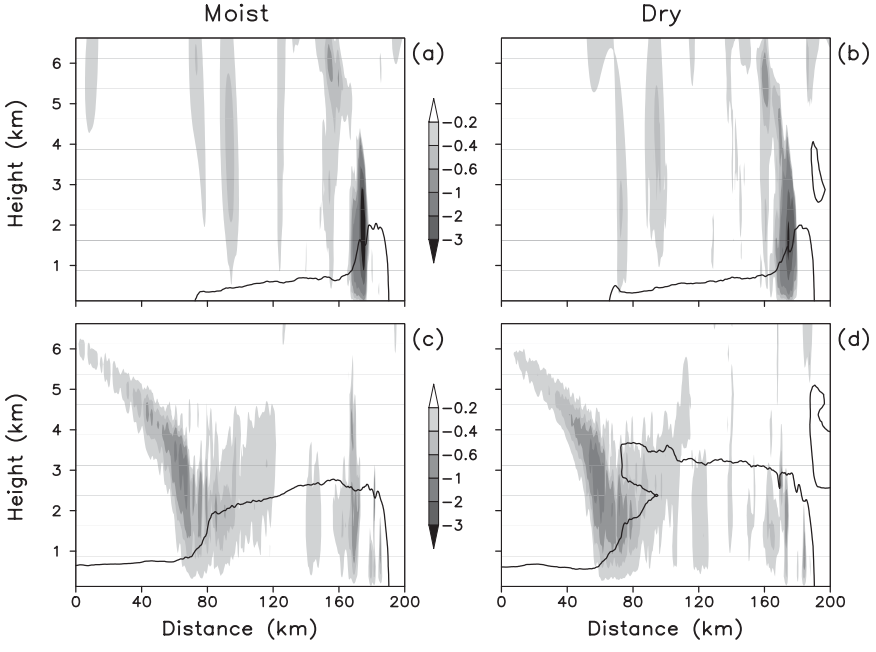

FIG. 12. As in Fig. 11, but for the line-type simulations having CAPE of 4500 J kg^{-1}.

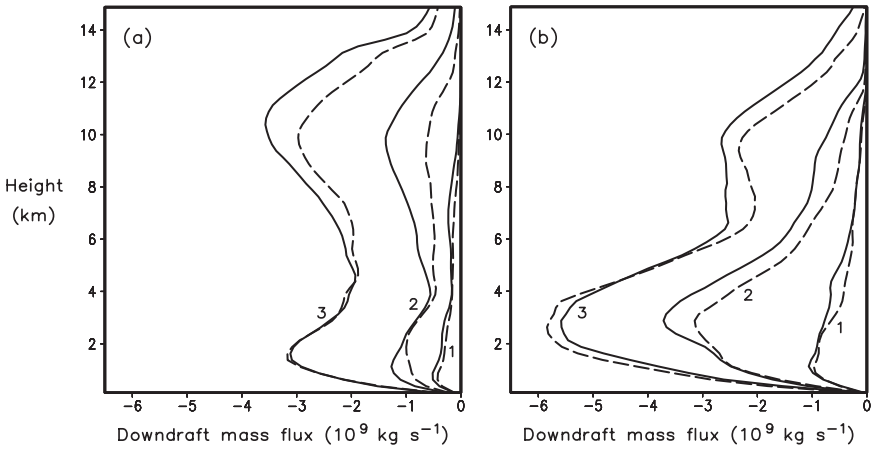

FIG. 13. As in Fig. 3, but for the downdraft mass flux.

owing to increased evaporation and sublimation of rain and snow. At 5 h, the enhancement of downdraft mass flux was maximized between 1 and 4 km AGL and between 110 and 150 km behind the gust front (Fig. 12). In the forward zone, in contrast, the high-CAPE downdraft mass flux was slightly reduced in strength when dry air was present.

The effect of dry air on the horizontally summed downdraft mass flux at all downdraft grid points is shown in Fig. 13. As in Cohen (2000), a grid point was classified as a downdraft point if the vertical velocity was less than -0.5 m s^{-1} and the total condensate mixing ratio was greater than 0.01 g kg^{-1}. In each simulation, the downdraft mass flux below 6 km AGL intensified over time as the stratiform region and its associated mesoscale downdraft developed. The enhancement of the downdraft mass flux in the high-CAPE simulation having dry air is clearly evident below 5 km AGL in Fig. 13b. However, at lower values of CAPE, and also in the early stages of the high-CAPE simulation, the downdraft mass flux was either unchanged or reduced in the drier environment.

The sensitivity of the simulated downdraft mass flux to dry air is consistent with the observed changes in the rates of diabatic cooling from condensate phase changes. The two primary zones of coherent downdraft formation were coincident with the locations of maximum along-line averaged diabatic cooling, which is illustrated for four primary phase changes in the high-CAPE simulations in Fig. 14. Downdrafts in the forward zone were generated by latent cooling from rain evaporation and hail melting, while cooling from snow sublimation, snow melting and rain evaporation contributed significantly to downdraft formation in the rearward zone. When dry air was present in the high-CAPE environment, the snow sublimation rate at 4 h was enhanced at the rear of the convective system, as snow fell into the layer of very dry air that was being drawn into the rear of the system. In the forward zone of downdrafts, the rain evaporation rate was slightly enhanced, but the hail melting rate was reduced. At times after 4 h, the enhancement of evaporation rates was less noticeable, and in the early stages of the high-CAPE simulations the diabatic cooling rates were little changed in the presence of dry air (not shown). At lower values of CAPE, the diabatic cooling rates were unchanged or reduced in the drier environments at all times.

To rigorously establish the magnitudes of diabatic cooling that were experienced by downdraft parcels arriving in the surface-based cold pool, backward trajectory calculations were computed for the high-CAPE simulations; this approach provides a Lagrangian confirmation of the ''snapshots'' of diabatic cooling in Fig. 14. An array of trajectories was initialized at 4 h at every grid point below 2.5 km AGL, over a horizontal area spanning the along-line dimension of the model domain and extending for 100 km in the across-line direction. The placement of the trajectory domain was designed to span the extent of the surface-based cold pool, in order to determine the history of the parcels that comprised the cold pool at 4 h. The trajectories were integrated backward for 30 min using model output that was preserved at a 60-s time interval. Figures 15a–d shows the along-line averaged diabatic cooling from rain evaporation and hail melting along the prior 30-min trajectory paths. As expected, the cooling from rain evaporation was enhanced in the drier environment in both the forward and rearward zones of downdraft formation. However, the cooling from hail melting in the forward zone was significantly reduced, and consequently the total diabatic cooling was not enhanced in the forward zone (Figs. 15e,f); this result is consistent with the

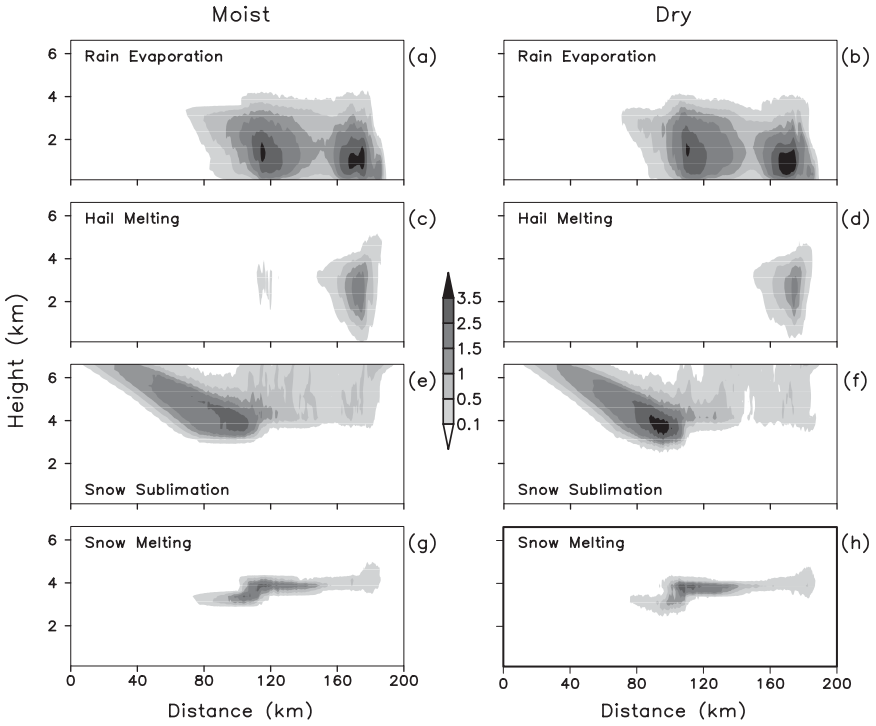

FIG. 14. Along-line average of the diabatic cooling rates (J kg^{-1} s^{-1}) from (a),(b) rain evaporation; (c),(d) hail melting; (e),(f) snow sublimation; and (g),(h) snow melting at 4 h in the (a),(c),(e),(g) moist and (b),(d),(f),(h) dry line-type simulations with CAPE of 4500 J kg^{-1}.

absence of downdraft mass flux enhancement in the forward zone.

The observed reduction in the hail melting rate in the drier environment is attributable to the reduction of the hail mixing ratio in association with the diminished updraft intensity. As discussed in section 3a(1), dry air aloft led to lower condensate mass for each hydrometeor species in every sensitivity test that was performed. In the case of rain evaporation and snow sublimation, the reduction in mixing ratios acted to partially offset the enhancement in cooling rates that would be expected in a drier environment. However, in the case of hail melting, lower humidity does not favor a greater melting rate, and thus the reduction in hail mass led directly to a diminished hail melting rate.

In the simulations having lower CAPE, the reduction in hydrometeor mass caused by dry air was more dramatic, and was sufficiently great to prevent any enhancement to diabatic cooling rates from lower humidity. Figure 16 shows that the domain-wide total rain evaporation was in fact reduced in the drier moderate-CAPE and low-CAPE environments. Thus, for CAPE of 3000 J kg^{-1} or lower, the reduction in convective intensity caused by dry air aloft was great enough to offset the favorable effects of dry air for downdraft development; however, for CAPE of 4500 J kg^{-1}, the convective intensity was hindered less, and dry air was able to cause the enhancement of downdrafts in the rearward zone.

The responses of the diabatic cooling rates and downdraft mass flux to dry air aloft were directly reflected in the strength of the surface-based cold pool in each simulation. As a robust measure of the cold pool strength, the parameter C^2 was used (Weisman 1992), which is proportional to the integrated negative buoyancy perturbation through the depth of the cold pool:

$$C^2 = -2g \int_0^D \left(\frac{\theta_\rho - \overline{\theta_\rho}}{\overline{\theta_\rho}} \right) dz, \tag{3}$$

where θ_ρ is the density potential temperature, defined as

$$\theta_\rho = \theta \left[\frac{1 + (q_v/\varepsilon)}{1 + q_t} \right], \tag{4}$$

where θ is the potential temperature. The parameter g is the acceleration due to gravity, D is the depth of the cold pool as defined by the upper limit of the -1-K potential temperature perturbation, and $\overline{\theta_\rho}$ is the base-state density potential temperature. Figures 17–19 depict C at 2 and 5 h, showing that the response of the cold pool

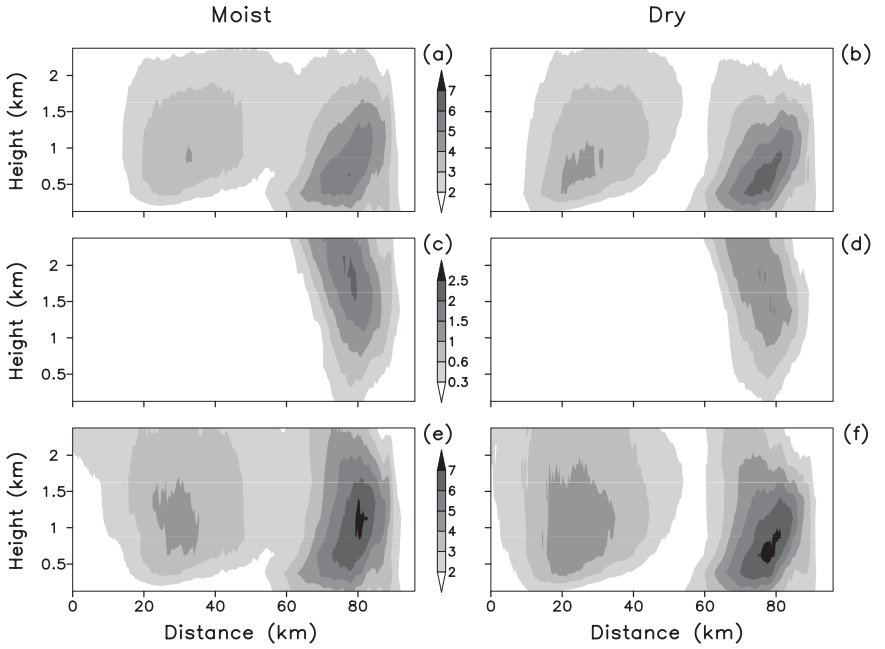

FIG. 15. Along-line average of the latent cooling (kJ kg^{-1}) from (a),(b) rain evaporation and (c),(d) hail melting and (e),(f) the total diabatic cooling (kJ kg^{-1}) from all phase changes over 30-min trajectory paths ending at 4 h in the (a),(c),(e) moist and (b),(d),(f) dry line-type simulations with CAPE of 4500 J kg^{-1}.

strength to dry air aloft was very similar to the response of the downdraft mass flux. In the high-CAPE environments, the presence of dry air caused enhancement of the cold pool strength more than 30 km behind the gust front at 5 h, in association with the enhanced diabatic cooling in the rearward zone of downdraft formation. However, *C* was largely unchanged within 30 km of the gust front, and was also very similar throughout the convective system at 2 h. For the moderate-CAPE simulations, the cold pool strength was reduced at most locations in the drier environment, except within 5 km of the gust front at 5 h, where little change was observed. When the CAPE was reduced to 1500 J kg^{-1}, *C* was generally unchanged or slightly reduced in the drier environment, in agreement with the modest weakening of the overall convective intensity and the downdraft mass flux.

b. Supercells

In both the moist and dry supercell simulations, the initially isolated updraft split into a pair of long-lived storms, the stronger of which propagated to the right of the mean wind in accordance with well-established theories of supercell development (Rotunno and Klemp 1982). After 90 min, the two storms were separated by 40–50 km, and a number of less intense convective cells had developed along the downshear side of the low-level outflow boundary produced by the storms. The region of low-level cold air generated by the convection covered an approximately circular area with a diameter of about 70 km (Fig. 20); however, the potential temperature perturbations within the cold pool were stronger and

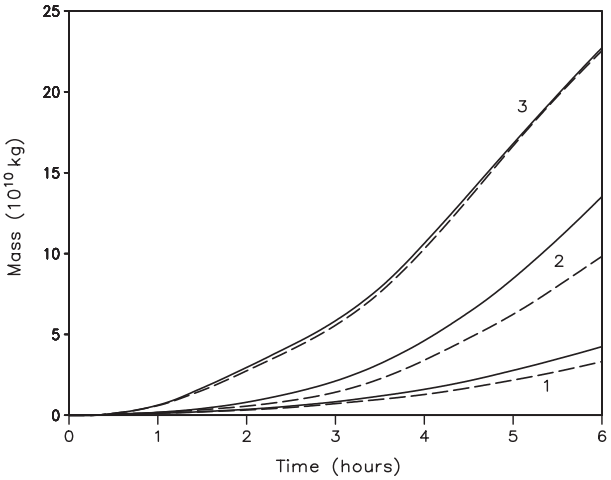

FIG. 16. Domain-wide total rain evaporation in the moist (solid lines) and dry (dashed lines) line-type simulations having CAPE of (1) 1500, (2) 3000, and (3) 4500 J kg^{-1}. For the dry simulation with CAPE of 1500 J kg^{-1}, the relative humidity in the dry layer was reduced to only 70%; the dry layers in the higher-CAPE simulations contained 10% relative humidity.

more expansive in the moist environment than in the environment having a dry layer.

When dry air was present, the stronger right-moving supercell was reduced in size and strength, as seen in the size of the midlevel updraft (Fig. 20), and in the intensity and spatial extent of the rain field reaching the ground (not shown). Figure 21 shows the horizontally summed updraft and downdraft mass fluxes at 1.5 h, calculated

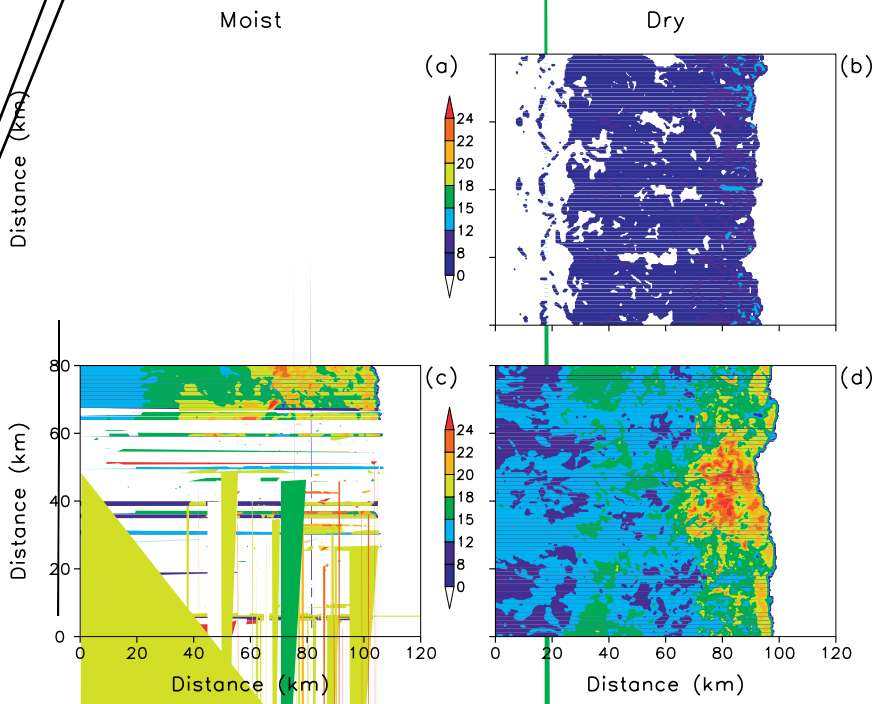

FIG. 18. As in Fig. 17, but for the line-type simulations having CAPE of 3000 J kg^{-1}.

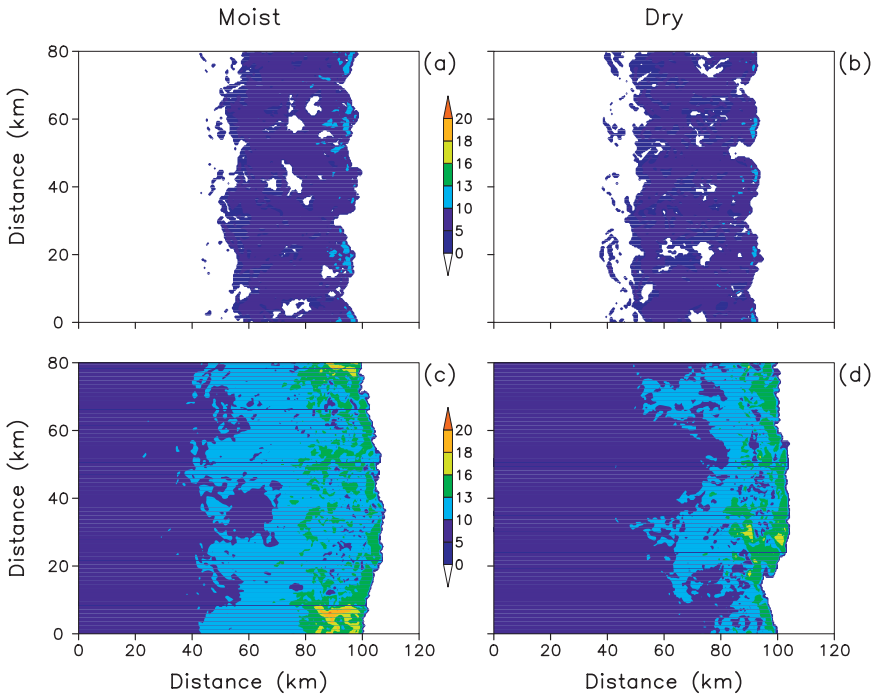

FIG. 19. As in Fig. 17, but for the line-type simulations having CAPE of 1500 J kg^{-1}. The dry layer in the dry simulation contained a minimum relative humidity of 70%.

using the same definition of updraft and downdraft points as in section 3a; the horizontal integration was performed only over the half of the model domain that contained the right-moving supercell. Clearly the supercell in the presence of dry air aloft was significantly weaker than the storm in the moist environment. Gilmore and Wicker (1998) hypothesized that dry air aloft may sometimes weaken a supercell updraft by generating stronger low-level outflow that propagates ahead of the storm, cutting off the low-level inflow of warm, moist air. This process did not occur in the simulations reported here; the primary midlevel updraft was located close to the low-level outflow boundary in both the moist and dry environments (Fig. 20). Moreover, the low-level outflow was weaker in the drier environment, both in terms of lowest-level potential temperature perturbation and cold

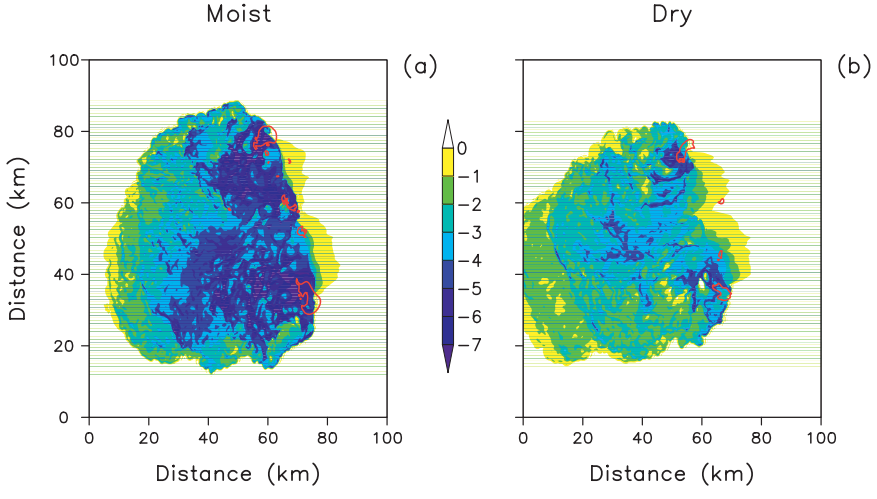

FIG. 20. Potential temperature perturbation (K, shaded) at 0.0625 km AGL, and the 20 m s^{-1} isopleth of vertical velocity (red line) at 6.0 km AGL, at 1.5 h in the (a) moist and (b) dry supercell simulations.

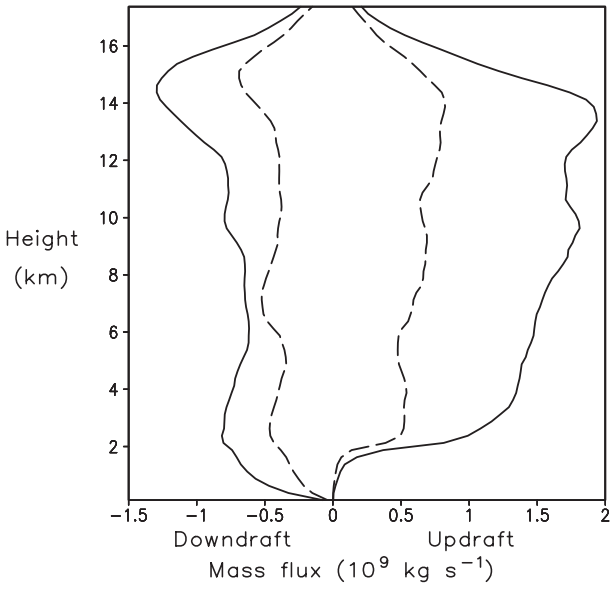

FIG. 21. Updraft (right two lines) and downdraft (left two lines) mass fluxes at 1.5 h in the moist (solid lines) and dry (dashed lines) supercell simulations. The horizontal summation was performed only over the half of the domain containing the right-moving supercell.

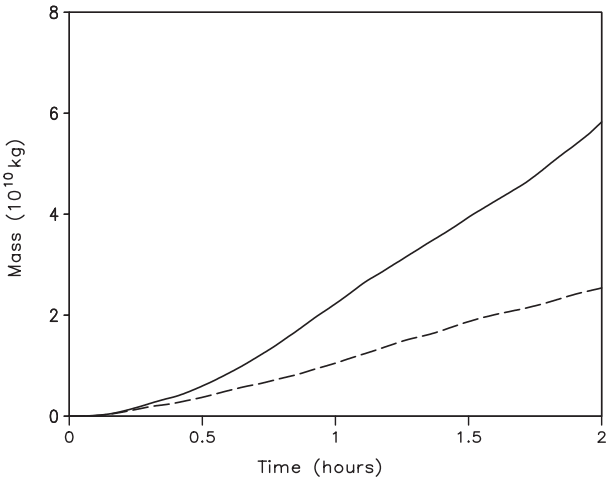

FIG. 22. Total condensate mass in the moist (solid line) and dry (dashed line) supercell simulations.

pool strength *C*. The observed weakening of the supercell in the drier environment was instead attributable to the effects of dry air on entrainment into the convective updraft, as in the line-type simulations. The domain-wide total mass of condensate was greatly reduced from as early as 20 min (Fig. 22), and the effect of the diminished entrainment was seen in the markedly reduced size of the primary updraft at midlevels (Fig. 20). Despite these effects, however, the domain-wide maximum vertical velocity, which occurred within the right-moving supercell, was almost unchanged when a dry layer was present, suggesting that nearly undiluted ascent was achieved in both the moist and dry environments.

The mechanisms contributing to weaker low-level outflow from the supercells in the drier environment were consistent with the processes discussed in section 3a. Figure 23 depicts the rates of rain evaporation and hail melting at 2 h; both the evaporation and hail melting were considerably smaller in the dry environment, in response to the reduction in rain and hail mixing ratios. Thus, in these supercell simulations the detrimental effects of dry air were sufficient to more than offset the favorable effects of dry air for evaporation rates, leading to smaller downdraft mass flux and weaker low-level outflow.

The experiments discussed here contrast strongly with the results of Gilmore and Wicker (1998), in which dry air aloft favored more intense low-level outflow. However, Gilmore and Wicker (1998) used a microphysics scheme similar to that of Kessler (1969), which excludes ice phase processes. To assess the significance of this difference, the supercell simulations were repeated with the Kessler scheme. Figure 24 presents the analogous results to Fig. 20, showing that the warm-rain microphysics scheme caused the outflow to be significantly enhanced when a dry layer was present. The right-moving storm in the drier environment was greatly reduced in strength, and was very disorganized, compared to the storm in the moist environment. Based on the relative locations of the primary updraft and the low-level outflow boundary, it appears that the intense outflow of cold air in the drier environment caused significant weakening of the supercell in the manner described by Gilmore and Wicker (1998). This result contrasts strongly with the mixed-phase simulations, in which the overall supercell intensity was hindered by the effects of dry air on entrainment rather than by excessively strong outflow.

In a further test of the microphysical sensitivity, a pair of supercell simulations was performed using the double-moment microphysics scheme of Morrison et al. (2009). Dawson et al. (2007, 2008) reported that supercell simulations using multi-moment schemes were able to better match observations by producing weaker and moister cold pools than when a single-moment scheme was used. However, in the simulations performed here, the double-moment supercell cold pools were considerably colder than those produced with the Goddard scheme (cf. Figs. 20 and 25), and were comparable in strength to those obtained with the Kessler scheme. As it is widely believed that the Kessler scheme produces cold pools that are too strong in the early stages of convective

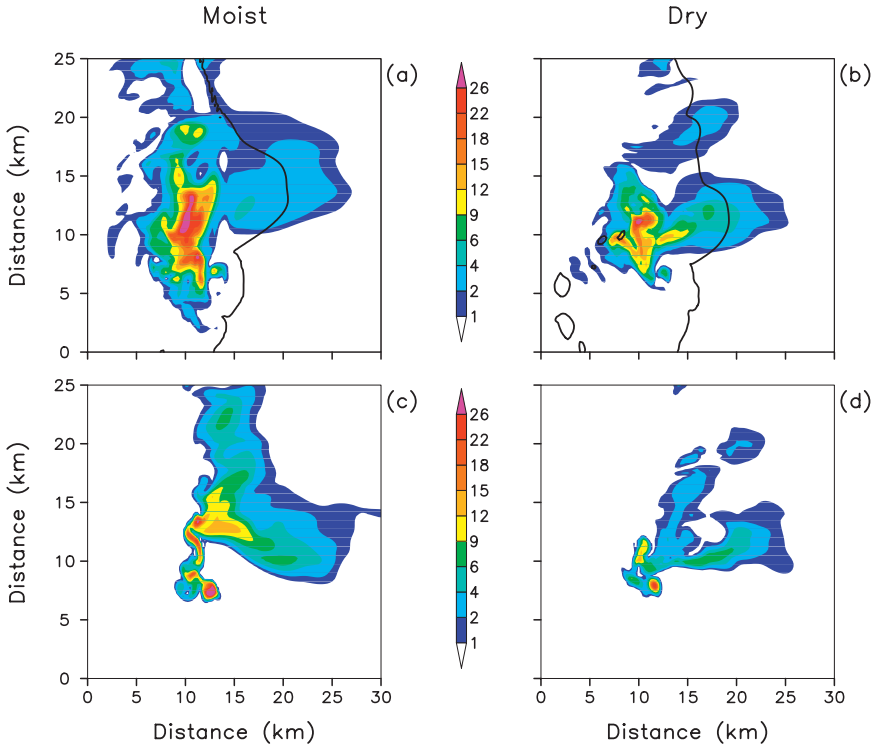

FIG. 23. (a),(b) Rain evaporation rate (J kg^{-1} s^{-1}) at 0.45 km AGL (shaded) and (c),(d) hail melting rate (J kg^{-1} s^{-1}) at 1.96 km AGL at 2 h in the (a),(c) moist and (b),(d) dry supercell simulations. These heights above ground represent the model levels at which (a),(b) the maximum rain evaporation rate and (c),(d) the maximum horizontally averaged hail melting rate were observed. The solid black line in (a),(b) depicts the −1 K potential temperature perturbation isopleth at 0.0625 km AGL at the same time.

activity (e.g., Trier et al. 1996), this result suggests that the utility of multi-moment schemes for supercell simulations must be examined further. Nevertheless, the results obtained with the Morrison scheme are consistent with the primary emphasis of this study, as the presence of dry air in the base-state sounding caused substantial weakening of the updraft and downdraft mass fluxes (not shown), and the cold pool intensity was little changed in

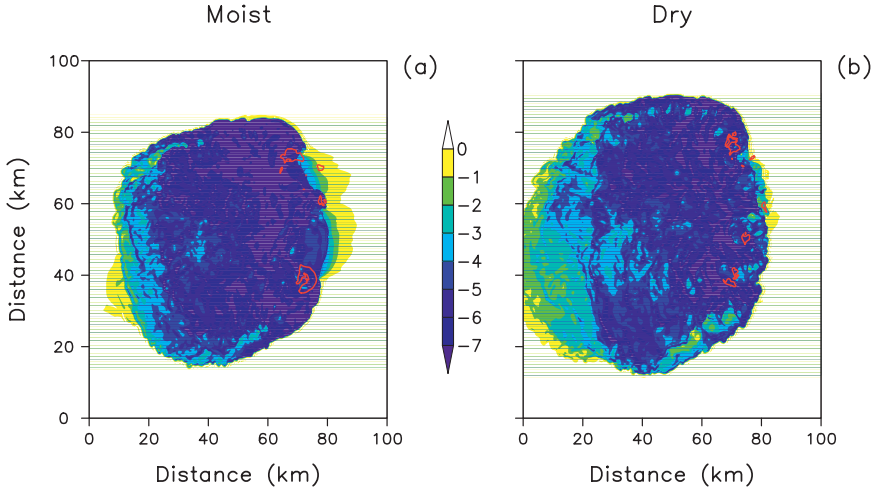

FIG. 24. As in Fig. 20, but for the supercell simulations using the Kessler microphysics scheme.

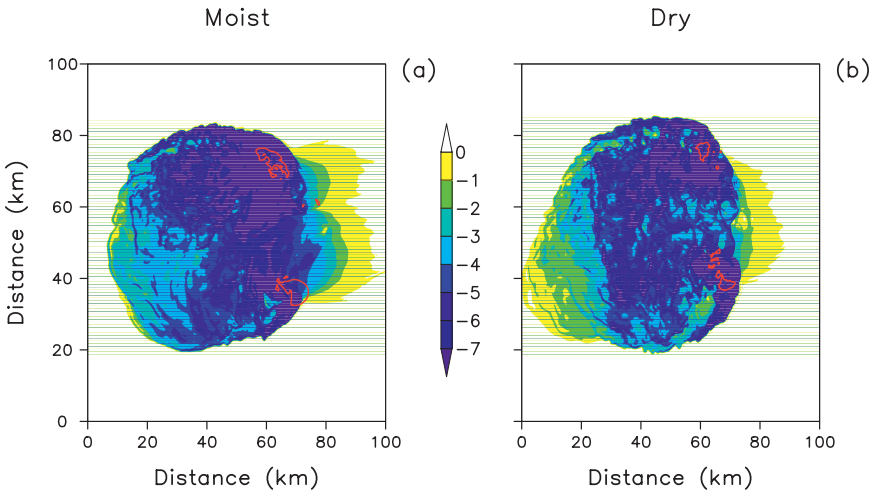

FIG. 25. As in Fig. 20, but for the supercell simulations using the Morrison double-moment microphysics scheme.

the right-moving storm, and was reduced in the left-moving supercell, when dry air was present.

c. *Additional experiments*

Using additional simulations of the quasi-linear convective mode, a number of further experiments was performed in which the sensitivity to dry air aloft was tested using a variety of different base-state and model setup parameters. A full description of the tests may be found in James (2009); a brief summary is offered herein.

The significance of the height of the dry layer was investigated by repeating the high-CAPE line-type simulations with the dry layer centered at 2.625 and 4.125 km AGL. In every other respect, the model setup was identical to the simulations described in section 3a. As the dry layer was moved to lower elevation, the reduction in total condensation, rainfall, and hydrometeor mass became slightly more pronounced, and the updraft and downdraft mass fluxes were reduced slightly more in the upper troposphere. The low-level mass fluxes did not show a strong sensitivity to the height of the dry air. However, the cold pool strength was enhanced more strongly in the rear of the convective system when the dry layer air was lower, but C was significantly reduced at the leading edge of the system (not shown).

An additional high-CAPE simulation was performed in which the relative humidity within the dry layer was reduced to only 50%, in order to test whether moderately dry air is more favorable than very dry air for downdraft and cold pool development. This hypothesis was not confirmed, as the response of the convection to the moderately dry air was very similar to, but less pronounced than, the response in the original test using relative humidity of 10%.

Finally, a variety of high-CAPE simulations was performed in which alternative mixed-phase microphysical parameterizations and different model numerics were employed. For these tests, the horizontal grid spacing was 1000 m, which allowed numerous experiments to be conducted in a brief period of time. In the microphysical sensitivity experiments, the schemes of Thompson et al. (2004) and Gilmore et al. (2004) were tested, as well as the ''graupel'' option of the Goddard scheme. The sensitivity to model numerics was tested by using sixth-order advection with an explicit filter having three different magnitudes of the nondimensional diffusion coefficient. Considerable variability in the details of the hydrometeor distributions was observed in these experiments, but the influence of dry air was qualitatively unchanged and did not contradict the results discussed in section 3a.

4. Discussion

According to the numerical results presented here, dry air above the cloud base exerts generally negative effects on convective intensity, owing to the decrease in updraft growth by entrainment. In the high-CAPE line-type simulations, dry air was found to enhance the downdraft mass flux and cold pool strength at the rear of the convective system, but at the leading edge of the convection, the downdraft intensity and cold pool strength were either unchanged or reduced in every sensitivity test. The model results therefore do not support the common perception that dry air aloft favors more intense low-level cold outflow. Given the unexpected nature of these results, a reexamination of previously published studies is warranted.

In the first widely cited attempt to predict the potential for severe wind gusts, Fawbush and Miller (1954) reported a strong correlation between wind gusts and a ''downrush temperature'' calculated by moist adiabatic descent from the wet-bulb freezing level. Similarly, Foster (1958) found a modest correlation between wind gusts and a calculated downdraft speed, which was obtained by assuming saturated descent from a midlevel wet-bulb adiabat. The latter result, in particular, has been interpreted to mean that drier air at midlevels produces stronger downdrafts (Gilmore and Wicker 1998). However, it is important to recognize that the correlations observed in these early studies may equally well have been produced by variations in midlevel temperature, and thus may simply reflect the well-known effect of CAPE on cold pool strength and outflow intensity.

More recent observational studies have focused on downdraft CAPE (DCAPE)[1] and the vertical gradient of θ_e as useful discriminants between nonsevere and severe wind-producing convective events. In an investigation of environmental conditions associated with derecho events, Evans and Doswell (2001) concluded that DCAPE is a reasonable proxy for cold pool strength, implying a causal connection between dry air aloft and enhanced low-level outflow strength. Atkins and Wakimoto (1991) and Cohen et al. (2007) found a strong connection between the vertical gradient of θ_e and the likelihood of severe low-level outflow, and they suggested that low humidity aloft was the key environmental parameter favoring strong downdrafts. In these studies, however, the influence of environmental humidity was not examined separately from the influence of CAPE. Both DCAPE and the vertical gradient of θ_e are highly correlated with CAPE, because the lapse rate between the surface and midlevels contributes significantly to the magnitude of each of these parameters; thus, it is impossible to rigorously conclude that dry air aloft was responsible for the observed correlations.

A recent investigation that addressed the ability of relative humidity alone to discriminate between ordinary and severe wind-producing convection was reported by Kuchera and Parker (2006). It was found that the minimum value of the relative humidity in the 2–4-km layer was slightly discriminating, and thus severe wind occurrence was slightly more likely, given the occurrence of convection, when drier air was present in the 2–4-km layer. However, Kuchera and Parker stated that ''other parameters seem to be more useful'' and that ''dry air in the midlevels is not uniquely associated with damaging winds.''

In studies that have documented the environments of derecho events, a moderately dry midtroposphere has often been observed, leading to frequent speculation that the damaging winds were partially attributable to the low humidity aloft (e.g., Johns and Hirt 1987; Duke and Rogash 1992; Bentley et al. 2000; Coniglio et al. 2004; Punkka et al. 2006). These studies have not demonstrated a causal relation, however. It is perhaps more likely that significant subsaturation aloft is commonly associated with an elevated mixed layer (Lanicci and Warner 1991), which in turn is correlated with increased lapse rates and higher CAPE. In this manner, dry air aloft may be symptomatic of an environment that is favorable for severe convection, though dry air itself does not enhance convective intensity.

Turning to the literature on tropical convection, a broad consensus is found that dry air aloft is detrimental to convective intensity. Strong evidence in this direction has emerged from the focus in recent years on the frequent occurrence of ''drought periods'' over the western Pacific warm pool. Studies such as Mapes and Zuidema (1996) and Lucas and Zipser (2000) have documented the variability of deep convective activity in this region in association with the presence or absence of synoptic-scale areas of dry air. During the periods of reduced humidity aloft, convection is widely suppressed, owing both to the detrimental effects of dry air on entrainment (Brown and Zhang 1997) and to increased convective inhibition (Parsons et al. 2000).

Several modeling studies have reproduced the inhibitory effects of dry air on tropical convection. For example, Lucas et al. (2000) reported simulations of convective systems that employed a base state derived from conditions observed in the Tropical Ocean and Global Atmosphere Coupled Ocean–Atmosphere Response Experiment (TOGA COARE) project. They found that increased moisture aloft was highly favorable for the intensity of their simulated squall lines, as measured by total condensation and rainfall; in addition, the cold pools were colder when the environment was more moist. Tompkins (2001) showed using a long-duration simulation of convection over the tropical ocean that the introduction of dry air to the convective environment above the cloud base greatly inhibited the convection. The presence of dry air was regarded as inhibiting convection both by reducing the humidity and therefore the CAPE in the boundary layer, and by reducing updraft buoyancy via entrainment.

In summary, the model results reported in this study are not inconsistent with previously documented observations. The results also do not undermine the well-established

[1] The definition of DCAPE and its properties are discussed by Gilmore and Wicker (1998).

concepts associated with downdraft formation in general. Beginning with studies such as Byers and Braham (1948) and Browning and Ludlam (1962), it has long been recognized that one of the primary features of deep convection is the evaporative cooling of potentially cold midlevel air, leading to downdraft development. The existence and dynamical importance of this process, being supported by a wide variety of studies, are not in question here. Rather, this study examines the effects of a *relatively moist or dry* environment on both updraft and downdraft processes, and concludes that a reinterpretation of the role of relatively dry air in midlatitude storms may be necessary.

5. Conclusions

Numerical simulations of both quasi-linear convective systems and supercells exhibited consistent sensitivity to varying humidity above the cloud base. Without exception, dry air aloft was found to reduce total condensation, total rainfall, and total mass of each condensate species. The updraft and downdraft mass fluxes were also reduced, except below 5 km in the high-CAPE line-type simulations. In the latter experiments, the downdraft mass flux at the rear of the stratiform region was enhanced in the presence of dry air, and the cold pool strength more than 30 km rearward of the gust front was modestly increased. However, the strength of the cold pool within its leading portion was either unchanged or reduced in all of the simulations having dry air aloft.

The influence of dry air was strongly sensitive to the environmental CAPE, with the detrimental effects of dry air for updraft entrainment and convective intensity being much greater at lower CAPE. This result was interpreted using the buoyancy-sorting model of entrainment, which suggests that the range of mixing fractions resulting in positive buoyancy is more greatly reduced by dry air when parcel buoyancy is low. Thus, convection at high values of CAPE is resistant to the effects of dry air, but low-CAPE convection is highly dependent on having a humid environment in order to grow by entrainment.

The sensitivity of the downdraft mass flux and cold pool strength to dry air aloft reflected the influence of dry air on the diabatic cooling rates associated with phase changes in the downdraft-forming regions. Although dry air aloft is directly favorable for rain and snow evaporation rates, the decline in hydrometeor mixing ratios in the drier environment exerted a negative tendency on the diabatic cooling rates. In all but the high-CAPE line-type simulations, an overall decline in diabatic cooling was observed, leading to reduced downdraft mass fluxes and reduced or unchanged cold pool strength. When high CAPE was used in the line-type simulations, the detrimental effects of dry air were less pronounced, and dry air was able to enhance the diabatic cooling rate, downdraft mass flux, and cold pool strength at the rear of the stratiform region. However, in the forward zone of downdraft formation, the decline in the hail melting rate offset the enhancement in the rain evaporation rate, leading to little net change in downdraft mass flux and cold pool strength.

The inclusion of the ice phase in the microphysical parameterization was discovered to be of profound importance to the observed sensitivity to dry air aloft. When a warm-rain scheme was employed, a dramatically different result was obtained wherein dry air aloft was beneficial to downdraft and outflow strength in environments of high CAPE. This sensitivity was observed in both the squall-line and supercell simulations, and reinforces the need to include ice phase microphysics in convection-resolving simulations.

The observed reduction in convective intensity when the environment contained dry air is consistent with prevailing conceptual models of convection over the tropical oceans. However, the failure of the simulated convection to generate enhanced low-level outflow in the presence of dry air is contrary to widely prevailing notions in the severe storms literature. Previous investigations of this topic were discussed, and it was shown that documented results do not unambiguously support the idea that dry air aloft generally intensifies downdrafts and low-level outflow. A particular tendency was noted for observational studies to address the role of environmental parameters that are affected by relative humidity, but that are also sensitive to CAPE, thus leaving open the possibility that the observed correlations simply reflect the effects of CAPE on cold pool and outflow strength.

Future investigation of the effects of dry air aloft on deep convection should include both modeling and observational components. Further modeling efforts should be directed toward the detailed assessment of more sophisticated microphysics schemes, including those that predict the number concentrations as well as the mass mixing ratios of hydrometeor species (e.g., Dawson et al. 2008; Morrison et al. 2009). Emphasis should also be placed on obtaining robust observational results that speak to the role of environmental humidity on convective processes. In future studies it is important that attempts be made to isolate the effects of relative humidity, as in Kuchera and Parker (2006), for example, rather than measuring environmental properties that do not have a unique relation to relative humidity. As in many previous research efforts, it is the combination of well-designed observational tests with an appropriate

modeling framework that will most rapidly advance the understanding of convective responses to dry air aloft.

Acknowledgments. The first author gratefully acknowledges the valuable encouragement and constructive criticism supplied by the members of his doctoral committee: Paul Markowski, Yvette Richardson, Mike Fritsch, Charlie Hosler, and Jonathan Mathews. Thought-provoking conversation with George Bryan, and useful comments from three anonymous reviewers, contributed to this investigation. This work was supported in part by the National Science Foundation (Award NSF ATM-0644533). Computing resources were supplied by the Department of Meteorology at The Pennsylvania State University and by the Scientific Computing Division of the National Center for Atmospheric Research (NCAR). Figures were constructed using the Grid Analysis and Display System (GrADS).

REFERENCES

Atkins, N. T., and R. M. Wakimoto, 1991: Wet microburst activity over the southeastern United States: Implications for forecasting. *Wea. Forecasting,* **6,** 470–482.

Bentley, M. L., T. L. Mote, and S. F. Byrd, 2000: A synoptic climatology of derecho producing mesoscale convective systems in the north-central Plains. *Int. J. Climatol.,* **20,** 1329–1349.

Braun, S. A., and W.-K. Tao, 2000: Sensitivity of high-resolution simulations of Hurricane Bob (1991) to planetary boundary layer parameterizations. *Mon. Wea. Rev.,* **128,** 3941–3961.

Brooks, H. E., C. A. Doswell III, and J. Cooper, 1994: On the environments of tornadic and nontornadic mesocyclones. *Wea. Forecasting,* **9,** 606–618.

Brown, R. G., and C. Zhang, 1997: Variability of midtropospheric moisture and its effects on cloud-top height distribution during TOGA COARE. *J. Atmos. Sci.,* **54,** 2760–2774.

Browning, K. A., and F. H. Ludlam, 1962: Airflow in convective storms. *Quart. J. Roy. Meteor. Soc.,* **88,** 117–135.

Bryan, G. H., 2002: An investigation of the convective region of numerically simulated squall lines. Ph.D. thesis, The Pennsylvania State University, 181 pp.

——, and J. M. Fritsch, 2002: A benchmark simulation for moist nonhydrostatic numerical models. *Mon. Wea. Rev.,* **130,** 2917–2928.

——, J. C. Knievel, and M. D. Parker, 2006: A multimodel assessment of RKW Theory's relevance to squall-line characteristics. *Mon. Wea. Rev.,* **134,** 2772–2792.

Byers, H. R., and R. R. Braham, 1948: Thunderstorm structure and circulation. *J. Meteor.,* **5,** 71–86.

Carr, F. H., and J. P. Millard, 1985: A composite study of comma clouds and their association with severe weather over the Great Plains. *Mon. Wea. Rev.,* **113,** 370–387.

Cohen, A. E., M. C. Coniglio, S. F. Corfidi, and S. J. Corfidi, 2007: Discrimination of mesoscale convective system environments using sounding observations. *Wea. Forecasting,* **22,** 1045–1062.

Cohen, C., 2000: A quantitative investigation of entrainment and detrainment in numerically simulated cumulonimbus clouds. *J. Atmos. Sci.,* **57,** 1657–1674.

Coniglio, M. C., D. J. Stensrud, and M. B. Richman, 2004: An observational study of derecho-producing convective systems. *Wea. Forecasting,* **19,** 320–337.

Dawson, D. T., M. Xue, J. A. Milbrandt, M. K. Yau, and G. Zhang, 2007: Impact of multi-moment microphysics and model resolution on predicted cold pool and reflectivity intensity and structures in the Oklahoma tornadic supercell storms of 3 May 1999. Preprints, *22nd Conf. on Weather Analysis and Forecasting/18th Conf. on Numerical Weather Prediction,* Park City, UT, Amer. Meteor. Soc., 10B.2.

——, ——, and ——, 2008: Improvements in the treatment of evaporation and melting in multi-moment versus single-moment bulk microphysics: Results from numerical simulations of the 3 May 1999 Oklahoma tornadic storms. Preprints, *24th Conf. on Severe Local Storms,* Savannah, GA, Amer. Meteor. Soc., 17B.4.

Deardorff, J. W., 1980: Stratocumulus-capped mixed layer derived from a three-dimensional model. *Bound.-Layer Meteor.,* **18,** 495–527.

Doswell, C. A., III, and P. M. Markowski, 2004: Is buoyancy a relative quantity? *Mon. Wea. Rev.,* **132,** 853–863.

Duke, J. W., and J. A. Rogash, 1992: Multiscale review of the development and early evolution of the 9 April 1991 derecho. *Wea. Forecasting,* **7,** 623–635.

Emanuel, K. A., 1994: *Atmospheric Convection*. Oxford University Press, 580 pp.

Evans, J. S., and C. A. Doswell III, 2001: Examination of derecho environments using proximity soundings. *Wea. Forecasting,* **16,** 329–342.

Fawbush, E. J., and R. C. Miller, 1954: A basis for forecasting peak wind gusts in non-frontal thunderstorms. *Bull. Amer. Meteor. Soc.,* **35,** 14–19.

Foster, D. S., 1958: Thunderstorm gusts compared with computed downdraft speeds. *Mon. Wea. Rev.,* **86,** 91–94.

Gilmore, M. S., and L. J. Wicker, 1998: The influence of midtropospheric dryness on supercell morphology and evolution. *Mon. Wea. Rev.,* **126,** 943–958.

——, J. M. Straka, and E. N. Rasmussen, 2004: Precipitation and evolution sensitivity in simulated deep convective storms: Comparisons between liquid-only and simple ice and liquid phase microphysics. *Mon. Wea. Rev.,* **132,** 1897–1916.

James, R. P., 2009: A numerical investigation of the effects of dry air aloft on deep convection. Ph.D. thesis, The Pennsylvania State University, 156 pp.

——, P. M. Markowski, and J. M. Fritsch, 2006: Bow echo sensitivity to ambient moisture and cold pool strength. *Mon. Wea. Rev.,* **134,** 950–964.

Johns, R. H., and W. D. Hirt, 1987: Derechos: Widespread convectively induced windstorms. *Wea. Forecasting,* **2,** 32–49.

——, and C. A. Doswell III, 1992: Severe local storms forecasting. *Wea. Forecasting,* **7,** 588–612.

Kain, J. S., and J. M. Fritsch, 1990: A one dimensional entraining/detraining plume model and its application in convective parameterization. *J. Atmos. Sci.,* **47,** 2784–2802.

Kessler, E., 1969: *On the Distribution and Continuity of Water Substance in Atmospheric Circulations. Meteor. Monogr.,* No. 32, Amer. Meteor. Soc., 84 pp.

Kingsmill, D. E., and R. A. Houze, 1999: Thermodynamic characteristics of air flowing into and out of precipitating convection over the west Pacific warm pool. *Quart. J. Roy. Meteor. Soc.,* **125,** 1209–1229.

Kirshbaum, D. J., G. H. Bryan, R. Rotunno, and D. R. Durran, 2007: The triggering of orographic rainbands by small-scale topography. *J. Atmos. Sci.,* **64,** 1530–1549.

Kuchera, E. L., and M. D. Parker, 2006: Severe convective wind environments. *Wea. Forecasting,* **21,** 595–612.

Lafore, J.-P., and M. W. Moncrieff, 1989: A numerical investigation of the organization and interaction of the convective and stratiform regions of tropical squall lines. *J. Atmos. Sci.,* **46,** 521–544.

Lanicci, J. M., and T. T. Warner, 1991: A synoptic climatology of the elevated mixed-layer inversion over the southern Great Plains in spring. Part I: Structure, dynamics, and seasonal evolution. *Wea. Forecasting,* **6,** 181–197.

Lin, Y.-L., R. D. Farley, and H. D. Orville, 1983: Bulk parameterization of the snow field in a cloud model. *J. Climate Appl. Meteor.,* **22,** 1065–1092.

Lucas, C., and E. J. Zipser, 2000: Environmental variability during TOGA COARE. *J. Atmos. Sci.,* **57,** 2333–2350.

——, ——, and B. S. Ferrier, 2000: Sensitivity of tropical west Pacific oceanic squall lines to tropospheric wind and moisture profiles. *J. Atmos. Sci.,* **57,** 2351–2373.

Mapes, B. E., 1993: Gregarious tropical convection. *J. Atmos. Sci.,* **50,** 2026–2037.

——, and P. Zuidema, 1996: Radiative-dynamical consequences of dry tongues in the tropical atmosphere. *J. Atmos. Sci.,* **53,** 620–638.

Markowski, P., and Y. Richardson, 2007: Observations of vertical wind shear heterogeneity in convective boundary layers. *Mon. Wea. Rev.,* **135,** 843–861.

McCaul, E. W., and M. L. Weisman, 2001: The sensitivity of simulated supercell structure and intensity to variations in the shapes of environmental buoyancy and shear profiles. *Mon. Wea. Rev.,* **129,** 664–687.

——, and C. Cohen, 2002: The impact on simulated storm structure and intensity of variations in the mixed layer and moist layer depths. *Mon. Wea. Rev.,* **130,** 1722–1748.

Morrison, H., G. Thompson, and V. Tatarskii, 2009: Impact of cloud microphysics on the development of trailing stratiform precipitation in a simulated squall line: Comparison of one- and two-moment schemes. *Mon. Wea. Rev.,* **137,** 991–1007.

Parsons, D. B., K. Yoneyama, and J.-L. Redelsperger, 2000: The evolution of the tropical western Pacific atmosphere-ocean system following the arrival of a dry intrusion. *Quart. J. Roy. Meteor. Soc.,* **126,** 517–548.

Punkka, A.-J., J. Teittinen, and R. H. Johns, 2006: Synoptic and mesoscale analysis of a high-latitude derecho-severe thunderstorm outbreak in Finland on 5 July 2002. *Wea. Forecasting,* **21,** 752–763.

Raymond, D. J., and A. M. Blyth, 1986: A stochastic mixing model for nonprecipitating cumulus clouds. *J. Atmos. Sci.,* **43,** 2708–2718.

Rotunno, R., and J. B. Klemp, 1982: The influence of the shear-induced pressure gradient on thunderstorm motion. *Mon. Wea. Rev.,* **110,** 136–151.

Thompson, G., R. M. Rasmussen, and K. Manning, 2004: Explicit forecasts of winter precipitation using an improved bulk microphysics scheme. Part I: Description and sensitivity analysis. *Mon. Wea. Rev.,* **132,** 519–542.

Thorpe, A. J., M. J. Miller, and M. W. Moncrieff, 1982: Two-dimensional convection in non-constant shear: A model of mid-latitude squall lines. *Quart. J. Roy. Meteor. Soc.,* **108,** 739–762.

Tompkins, A. M., 2001: Organization of tropical convection in low vertical wind shears: The role of water vapor. *J. Atmos. Sci.,* **58,** 529–545.

Trier, S. B., W. C. Skamarock, M. A. LeMone, D. B. Parsons, and D. P. Jorgenson, 1996: Structure and evolution of the 22 February 1993 TOGA COARE squall line: Numerical simulations. *J. Atmos. Sci.,* **53,** 2861–2886.

Weisman, M. L., 1992: The role of convectively generated rear-inflow jets in the evolution of long-lived mesoconvective systems. *J. Atmos. Sci.,* **49,** 1826–1847.

——, and J. B. Klemp, 1982: The dependence of numerically simulated convective storms on vertical wind shear and buoyancy. *Mon. Wea. Rev.,* **110,** 504–520.

——, and R. Rotunno, 2000: The use of vertical wind shear versus helicity in interpreting supercell dynamics. *J. Atmos. Sci.,* **57,** 1452–1472.

——, J. B. Klemp, and R. Rotunno, 1988: Structure and evolution of numerically simulated squall lines. *J. Atmos. Sci.,* **45,** 1990–2013.

Wicker, L. J., and W. C. Skamarock, 2002: Time-splitting methods for elastic models using forward time schemes. *Mon. Wea. Rev.,* **130,** 2088–2097.

Zipser, E. J., 1977: Mesoscale and convective-scale downdrafts as distinct components of squall-line structure. *Mon. Wea. Rev.,* **105,** 1568–1589.